A comprehensive DNS database to investigate measures of roughness and LES wall models

By M. MacDonald†, D. Chung†, N. Hutchins†, L. Chan†, A. Ooi†, G. I. Park AND B. Pierce

A comprehensive direct numerical simulation (DNS) database of turbulent pipe flow was used to investigate the physics of turbulent flow over three-dimensional roughness, with an eye toward developing multiscale wall models for large-eddy simulation (LES). Using cases in which the height of the roughness was varied, we characterize, at various levels of granularity, the body forces that would be exerted by a wall model. This body force is cast as a non-dimensional drag coefficient, which shows an exponential decay form. Moreover, the drag coefficient was found to have very similar behavior at the two Reynolds numbers tested, $\mathrm{Re}_\tau = 180$ and $\mathrm{Re}_\tau = 540$ for matched roughness Reynolds numbers. This drag coefficient was then imposed as a body force in a DNS of turbulent flow over a smooth wall at $\mathrm{Re}_\tau = 180$ to study the detail to which the body forces need to be represented in order to recover the first- and second-order statistics. These results from the roughness model show promising agreement when compared with the DNS of the actual gridded roughness. Time-averaged flow structures are also compared to those in the gridded roughness cases, with the model for the finest filter scale tested showing reasonable qualitative agreement.

1. Introduction

Most engineering and atmospheric flows are over hydrodynamically rough surfaces. The central question in roughness research is to be able to relate the shape of the roughness, which is a purely geometrical property, to its dynamical effect (such as drag) without conducting expensive or even impossible experiments or simulations (Flack & Schultz 2010). The difficulty is compounded when used in the context of large-eddy simulation (LES). LES is a promising tool for predicting turbulent flows but the fidelity of its prediction is hampered by the wall model component, which relates the shear stress (or drag per unit area) to the resolved flow conditions above it.

Current wall models employed in roughness studies generally modify either the boundary conditions on the wall or the Navier–Stokes equations close to the wall. In particular, Busse & Sandham (2012) (hereby referred to as BS12) modified the Navier–Stokes equations to introduce a forcing term in the near-wall region, with the results showing the same general trends that are seen in experimental roughness studies. A range of different assumed forcing profiles was investigated, however no experimental or theoretical justification for them was given. In this study, the roughness model based on the work of BS12 is used; however the forcing term is given in terms of a non-dimensional force coefficient, similar to the drag coefficient suggested in Raupach *et al.* (1991). The force coefficient is obtained from a direct numerical simulation (DNS) database of turbulent pipe flow over a systematically varied rough wall (Chan *et al.* 2014). The results from

† Department of Mechanical Engineering, University of Melbourne, Australia

the roughness-model DNS can then be compared with the exact gridded-roughness DNS. This aspect of the study is therefore a validation of the forcing term approach, using DNS to isolate numerical and subgrid-scale effects present in LES.

Nakayama *et al.* (2004) utilize a similar method in that body forces are used to represent unresolved roughness in LES. The effects of roughness can be described by two body forces in the Navier–Stokes equations, which are needed to represent the complex dynamic effects of roughness. These forces are the result of the form (or pressure) and skin-friction (or viscous) components of drag that the roughness exerts on the fluid, namely

$$\mathbf{P} = \iint_S \mathcal{G}(\boldsymbol{x}, \boldsymbol{\xi}; \Delta) \frac{p(\boldsymbol{\xi}) - \langle p_{surf} \rangle}{\rho} \boldsymbol{n} \, \mathrm{d}S_\xi, \qquad \mathbf{T} = \iint_S \mathcal{G}(\boldsymbol{x}, \boldsymbol{\xi}; \Delta) \nu \frac{\partial \boldsymbol{u}}{\partial n}(\boldsymbol{\xi}) \, \mathrm{d}S_\xi, \quad (1.1)$$

where $\mathcal{G}$ is the fluid-volume-weighted filter, n is the outward unit normal vector of the rough boundary S, $\boldsymbol{\xi}$ is the dummy integration variable, Δ is the filter width, and $\langle p_{surf} \rangle$ is the mean surface pressure. Nakayama *et al.* use a single, assumed value for the skin friction and form drag coefficients, C_f and C_d, to model the $\mathbf{T}$ and $\mathbf{P}$ terms, respectively. A dynamic procedure to determine these coefficients is presented, although no evaluation of it is performed. In this study, we are using the drag coefficient obtained from the gridded-roughness DNS, which is then used directly in the roughness model simulations. Moreover, the roughness used in this study is three-dimensional, whereas Nakayama *et al.* used two-dimensional roughness. De Marchis & Napoli (2012) pointed out that real roughness is usually three-dimensional in nature, which can have different flow behavior from that observed over two-dimensional roughness.

Another aspect of the roughness model that needs to be considered is the effect of the filter width. If λ is some characteristic length of the roughness, then λ/Δ determines if the roughness is resolved by the LES simulation, $\lambda/\Delta < 1$, or is unresolved, $\lambda/\Delta > 1$. It is often the case in practical applications that all of these regimes are present simultaneously, in the form of multiscale roughness. The effect of varying filter scales in representing the roughness drag coefficient is examined at various levels for unresolved roughness. It is of interest to analyze the level of detail that is required by the model to faithfully reproduce the dynamic effects of roughness. Understanding the dynamical effects and secondary flows is particularly important in studies of heat flow, wildfires, and tree spore dispersal in plant canopies. Moreover, the proposed roughness model at varying filter lengths can provide valuable fundamental information into the causes of observed roughness behavior. In particular, understanding the level of detail required in the forcing term will hopefully motivate future models.

It is important to stress that the current modeling approach is different from the immersed boundary (IB) method commonly used in roughness studies (e.g., Bhaganagar *et al.* 2004; Orlandi & Leonardi 2006). In the IB method, the impermeability and no-slip boundary conditions are enforced by applying a unique forcing value to each cell that is determined formally as a procedure in the numerical scheme. This requires exact information on the roughness topology to enforce the boundary conditions. In the current roughness model, a statistically averaged forcing term is applied as part of an analytical scheme taken from classical turbulence-modeling phenomenology. The latter scheme lends itself more readily to current current wall models in the literature, such as Wang & Moin (2002) and Park & Moin (2014), where the roughness model is simply an additional term in the wall model. A related method was used in the force calculation for particulate flow in Apte (2004).

2. Methodology

Direct numerical simulations have been conducted for turbulent pipe flow at $\mathrm{Re}_\tau = 180$ and, for the gridded (body-fitted) roughness, also at $\mathrm{Re}_\tau = 540$. The unstructured second-order finite volume code CDP was used in simulations of both the gridded roughness and the smooth wall with roughness model.

2.1. *Gridded-roughness DNS*

Gridded-roughness simulations were performed prior to the commencement of the summer program, in which the roughness was defined by a three-dimensional sinusoidal surface

$$R(x,\theta) = R_0 + h\cos\left(2\pi x/\lambda_x\right)\cos\left(2\pi R_0\theta/\lambda_s\right), \tag{2.1}$$

where R_0 is the reference radius of the pipe, h the mean-to-peak height (semi-amplitude) of the roughness, and λ_x and λ_s the wavelengths of the roughness elements in the streamwise and azimuthal (as an arc length $s = r\theta$) directions, respectively. In all cases, the azimuthal wavelength is kept the same as the streamwise wavelength, $\lambda_x = \lambda_s = \lambda$. The amplitude and wavelength of the gridded roughness is varied systematically for $2.5 \leq h^+ \leq 20$ and $113 \leq \lambda^+ \leq 283$ with the full details given in Chan *et al.* (2014). Cases involving the gridded roughness are referred to by their amplitude and wavelength, $h^+\_\lambda^+$. For example, case 10_141 has an amplitude of $h^+ = 10$ and wavelength $\lambda^+ = 141$. The roughness model will be using only two cases from this database in which the amplitude is varied from $h^+ = 10$ to $h^+ = 20$ for $\lambda = 141$ (cases 10_141 and 20_141).

When building a suitable roughness wall model for LES, characterization from the gridded-roughness DNS is first performed. The force that is exerted by the rough wall onto the fluid is made non-dimensional into a local force coefficient, which varies with wall-normal position $y = (R_0 - r)/R_0$. Here, the trough of the roughness is located at $y^+ = -h^+$ and the crest at $y^+ = h^+$. The ith component of the force coefficient is

$$C_{D,i}(y,\Delta) = \frac{\overline{F_{D,i}}(y,\Delta)}{\frac{1}{2}\rho\langle U_x^\beta(y,\Delta)\rangle^2 A_w(y,\Delta)}, \tag{2.2}$$

where $\overline{F_{D,i}}$ is the time-averaged ith component of the force that the solid rough wall exerts on the fluid (both viscous and pressure forces), acting over the filter box of size Δ. In the case of the streamwise direction, this is simply the drag force and hence we have defined the local drag coefficient. A_w is the projected wall-normal area of the roughness element whereas $\langle U_x^\beta\rangle$ is the time-averaged streamwise velocity, spatially averaged over Δ. Owing to the unstructured grid, spatial averages of quantities are performed within a thin wall-normal annulus using a fluid-volume weighting. The spatial average of some quantity σ inside the ith annulus, Ω_i is $\langle\sigma^\beta\rangle_i = \sum_{j\in\Omega_i}\sigma_j V_j \Big/ \sum_{j\in\Omega_i} V_j$, where V_j is the volume of the cell j inside the annulus Ω_i (Figure 1 (b)). Note that the force is not averaged but will be the total force acting within the annulus. In the gridded-roughness DNS, the spatial averaging operation is over only fluid-filled cells in Ω_i, hence $\langle U_x^\beta\rangle$ is an intrinsic spatial average denoted by the superscript β. The alternative spatial averaging technique is termed the superficial average (denoted with superscript γ), in which the solid regions of the domain are included in the average. If $\varepsilon(y)$ is the ratio of the fluid to solid volumes, where $\varepsilon = 1$ in fully fluid regions and $\varepsilon = 0$ in fully solid regions, then the superficial velocity and intrinsic velocity are related by $u^\gamma = \varepsilon u^\beta$ (Breugem & Boersma 2005). Unless otherwise stated, all velocities will refer to their superficial average form and the superscript γ will be dropped.

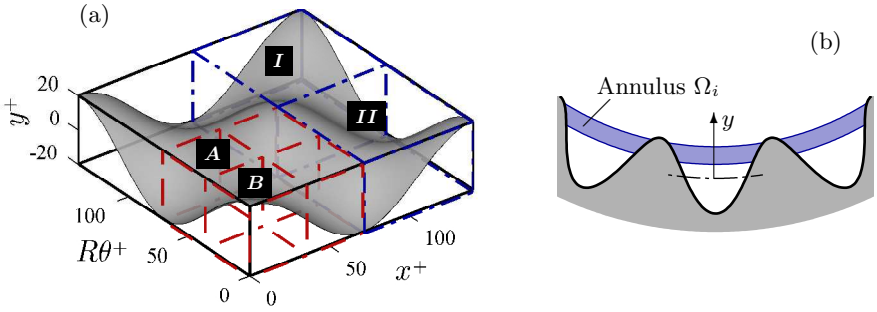

FIGURE 1: (a) Single sinusoidal roughness element of case 20_141, with three different filter box sizes; $\Delta_1 = \lambda$ (——), $\Delta_2 = \frac{1}{2}\lambda$ (— · —), and $\Delta_3 = \frac{1}{4}\lambda$ (— —). (b) Sketch of averaging annulus in the cross-sectional plane. Dash dotted line shows $y = 0$.

As discussed above, an important parameter to consider is the filter length Δ and its relation to the roughness wavelength λ. Figure 1 (a) shows a single sinusoidal roughness element of the gridded-roughness case 20_141 and the different filter lengths considered in this study. The largest filter length, $\Delta_1 = \lambda$, results in a streamwise drag coefficient that only depends on y, whereas the azimuthal coefficient is zero due to symmetry. There is a small viscous drag component that acts in the negative radial direction; however this is usually only 5–10% that of the streamwise drag coefficient. The next filter length is $\Delta_2 = \frac{1}{2}\lambda$, which has the same form for $C_{D,x}$ and $C_{D,r}$ as with Δ_1 due to the symmetry of the four quadrants. However, this filter length now introduces a spatially varying azimuthal coefficient depending on which quadrant the element is in; the filter boxes I and II in Figure 1 have oppositely signed but equal magnitude azimuthal forcing. The final filter length which is analyzed is $\Delta_3 = \frac{1}{4}\lambda$. Here, all three force coefficients as well as ε vary in space. In particular, filter box A in Figure 1 (a) is entirely fluid ($\varepsilon = 1$) for $0 \leq y^+ \leq h^+$ and no forcing is applied. The alternative filter box B has ε varying from 1 at the crest to 0 at $y^+ = 0$.

2.2. *Roughness-modeled DNS*

In the roughness model simulations, the force coefficient is applied as a body force term in the Navier–Stokes equations. The equations which are being solved are similar to those of Nakayama *et al.* (2004),

$$\nabla \cdot \widetilde{\mathbf{u}}^\beta = \chi \widetilde{u}_{\widetilde{n}}^\beta, \tag{2.3}$$

$$\frac{\partial \widetilde{\mathbf{u}}^\beta}{\partial t} + \nabla \cdot (\widetilde{\mathbf{u}^\beta \mathbf{u}^\beta}) = -\frac{1}{\rho}\nabla \widetilde{p}^\beta + \nabla \cdot (\nu \nabla \widetilde{\mathbf{u}}^\beta - \nu \chi \widetilde{\mathbf{u}}^\beta \widetilde{\mathbf{n}} - \tau) + \mathbf{P} + \mathbf{T} + \chi \left(\widetilde{\mathbf{u}^\beta u_{\widetilde{n}}^\beta} - \nu \frac{\partial \widetilde{\mathbf{u}}^\beta}{\partial \widetilde{n}} \right), \tag{2.4}$$

Here, the authors use the filter function $\mathcal{G}$ to define the filtered, intrinsic flow variables of velocity $\widetilde{\mathbf{u}}^\beta$ and pressure $\widetilde{p}^\beta$. The filter $\mathcal{G}$ depends on a fluid-weighting function $W(\boldsymbol{x})$ (see Figure 1 in Nakayama *et al.* (2004) for further clarification), from which the parameter $\chi = \nabla W / W$ is defined. However, if the flow variables are instead solved in superficial form, that is, the domain is entirely fluid and W is constant in space, then $\nabla W = \chi = 0$. Moreover, in order to isolate numerical and subgrid-scale effects and focus solely on the roughness model, DNS is performed so that the subgrid-scale stress $\tau = 0$. Hence, the continuity and conservation of momentum equations being solved in the roughness-

modeled DNS are

$$\nabla \cdot \mathbf{u} = 0, \qquad \frac{\partial \mathbf{u}}{\partial t} + \nabla \cdot (\mathbf{uu}) = -\frac{1}{\rho}\nabla p + \nabla \cdot (\nu \nabla \mathbf{u}) + \mathbf{G} + \mathbf{K}, \tag{2.5}$$

where $\mathbf{G} = G_x \mathbf{i}$ is the uniform, time-varying streamwise forcing term required to maintain constant mass flux through the pipe, and $\mathbf{K} = \mathbf{P} + \mathbf{T}$ is the roughness model forcing term. Here, the term DNS is used in the context of maintaining adequate DNS-like grid spacing, so that the subgrid scale stress is zero. The roughness model is applied to the flow through a smooth-wall pipe, so that if the roughness model was disabled ($\mathbf{K} = \mathbf{0}$) then smooth-wall DNS of turbulent flow is obtained. A pipe geometry is used as the gridded-roughness DNS in Chan *et al.* (2014) also uses a pipe. Compared with the gridded-roughness DNS, the smooth-wall grid has almost half as many cells.

The forcing term $\mathbf{K}$, based on the force coefficients, is determined from the gridded rough wall DNS (Eq. 2.2). This forcing is added as a momentum sink during the prediction step of the pressure-correction method. The ith component of force is applied to cell j as

$$K_{i,j} = \frac{C_{D,i}}{V}\frac{1}{2}\rho A_w \frac{u_{x,j}}{\varepsilon}\left|\frac{u_{x,j}}{\varepsilon}\right| V_j, \tag{2.6}$$

The form of the instantaneous streamwise velocity $u_x|u_x|$ is used as it always ensures a damping effect of the drag force (BS12). V_j is the volume of cell j whereas V is the total volume of the annulus used to calculate $C_{D,i}$. Recall that $C_{D,i}$ is defined using the rough wall intrinsic velocity, however the velocity being solved for in the smooth wall model simulation, $u_{x,j}$, is the superficial velocity. This velocity must therefore be cast in its intrinsic form by dividing by ε. Compared with the gridded-rough-wall case, the forcing term is applied from the virtual wall (mean roughness height), $y^+ = 0$, to the roughness crest at $y^+ = h^+$. The trough of the roughness ($y^+ = -h^+$ to $y^+ < 0$) is not represented by this roughness model. It is assumed that the force exerted below the virtual wall in the gridded roughness case can be approximated by the viscous shear stress that is applied to the virtual wall in the model simulation. This approximation will be investigated below. It was necessary to artificially reduce the instantaneous forcing value as it could become very large for small values of ε and produce an instability in the flow. This involved clipping the $K_{i,j}$ term, so that when $K_{i,j} > \zeta$ it was set to have value ζ, which was approximately 500 times larger than the mean forcing value.

3. Results

The gridded-roughness and roughness-model DNS cases that were performed are outlined in Table 1. Note that some of the roughness model simulations use the same symbols for different roughness amplitudes; however all figures involving the roughness model simulations will contain only the one amplitude.

3.1. *Drag coefficient*

The streamwise drag coefficient obtained from the gridded roughness cases 10_141 and 20_141 is shown in Figure 2 where the filter length is just the wavelength of the roughness, $\Delta_1 = \lambda$. This filter length means that $C_{D,x}$ varies only in y with no dependence on the azimuthal or streamwise directions. Also shown is the drag coefficient at $\mathrm{Re}_\tau = 540$ for the same roughness Reynolds numbers (matched h^+, but R_0/h changes). The drag coefficient shows an exponential decay. Both cases 10_141 and 20_141 exhibit a similar trend, which suggests a generalized form for C_D could be developed. Moreover, it can be

Gridded (body-fitted) roughness DNS cases

ID	Symbol	Re_τ	h^+	R_0/h	λ_x^+
Smooth	⊙	180	-	-	-
10_141	◀	180	10	18	141
540.10_141	▶	540	10	54	141
20_141	★	180	20	9	141
540.20_141	✸	540	20	27	141

Roughness-model DNS cases

ID	Symbol	Re_τ	h^+	Δ
10_141_Δ_1	■	180	10	λ
10_141_Δ_2	●	180	10	$\frac{1}{2}\lambda$
10_141_Δ_3	◆	180	10	$\frac{1}{4}\lambda$
20_141_Δ_1	■	180	20	λ
20_141_Δ_2	●	180	20	$\frac{1}{2}\lambda$
20_141_Δ_3	◆	180	20	$\frac{1}{4}\lambda$

TABLE 1: Description of the different simulations conducted. h^+ is the roughness mean to peak amplitude, R_0 is the mean pipe radius, λ_x^+ is the wavelength, and Δ is the filter width (see Figure 1) used to define $C_{D,i}$ in the roughness model simulation.

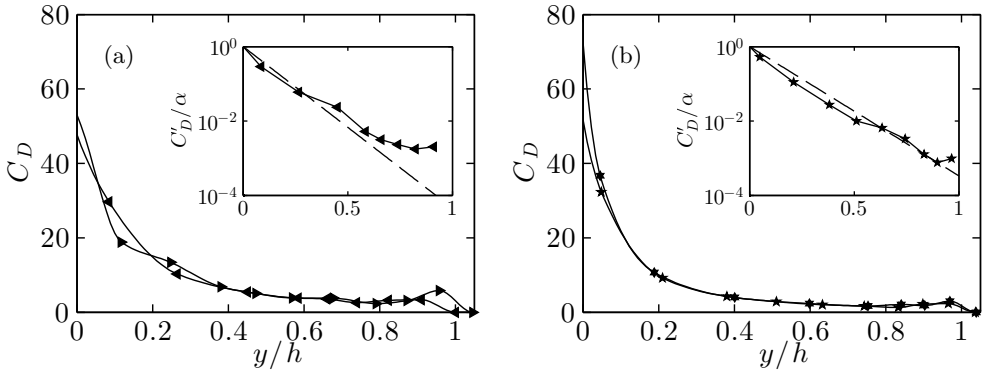

FIGURE 2: Streamwise drag coefficient C_D against wall-normal position normalized on roughness semi-amplitude y/h, starting from the mean roughness height location $y = 0$. Data obtained from simulations of gridded-roughness DNS, see Table 1. (a) Roughness amplitude $h^+ = 10$ at $\mathrm{Re}_\tau = 180$ (◀) and $\mathrm{Re}_\tau = 540$ (▶); (b) roughness amplitude $h^+ = 20$ at $\mathrm{Re}_\tau = 180$ (★) and $\mathrm{Re}_\tau = 540$ (✸). Using filter width $\Delta_1 = \lambda$. Inset shows exponential forcing term of BS12 (— —) with $h^+_{BS12} = 1$ in (a) and $h^+_{BS12} = 2.5$ in (b), and the appropriately scaled drag coefficient C_D'/α for $\mathrm{Re}_\tau = 180$ (see text).

seen that there is almost no variation in C_D for both cases at the two different Reynolds numbers. This suggests that simulations of gridded rough surfaces could be conducted at low Reynolds numbers to obtain C_D, which is then inputted into the proposed model and performed at a higher Reynolds numbers. BS12 investigated a similar forcing model in the form of $\alpha F(h^+_{BS12})u_x|u_x|$, and tried an exponential form for $F(h^+_{BS12})$, where h^+_{BS12} was an integral height parameter. The insets of Figure 2 show the drag coefficient C_D'/α when scaled in the same form as F of BS12, with α selected so that $C_D'(y = 0)/\alpha = 1$. For both gridded-roughness cases at $\mathrm{Re}_\tau = 180$, α was around 37. However, BS12 investigated this exponential forcing term for only $h^+_{BS12} = 2.5$ and larger, with $\alpha = 1$. The current forcing term is therefore much stronger in magnitude than BS12, but distributed closer to the wall. The scaled C_D' does show a reasonable exponential trend, however, and appears to to rise above the exponential dashed line toward the crest of the roughness.

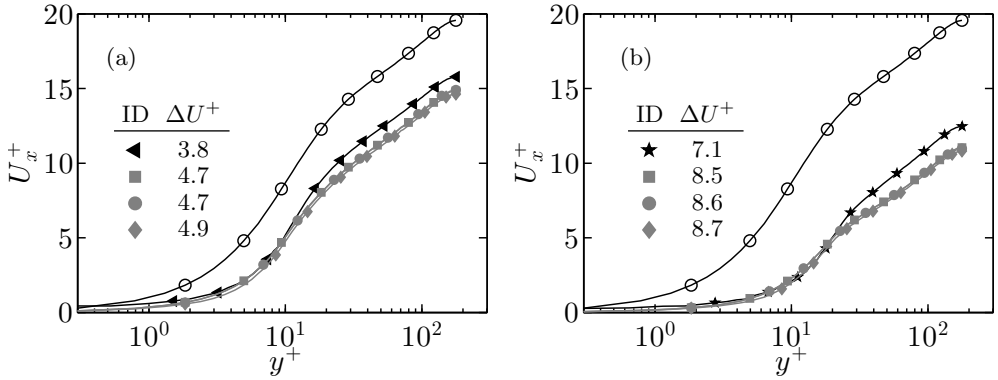

FIGURE 3: Mean streamwise velocity profile comparing the gridded-roughness DNS with the roughness-model DNS. (a) Amplitude $h^+ = 10$, (b) amplitude $h^+ = 20$. Symbols: (⊙): smooth-wall DNS, (◀): gridded 10_141, (★): gridded 20_141. Roughness model with filter lengths $\Delta_1 = \lambda$ (■), $\Delta_2 = \frac{1}{2}\lambda$ (●), $\Delta_3 = \frac{1}{4}\lambda$ (♦), for each amplitude. Roughness function ΔU^+ is shown for each case in the appropriate table.

3.2. *Time-averaged statistics*

The drag coefficient obtained from the gridded roughness is used in the roughness-model DNS for flow over a smooth wall. The velocity profiles for the smooth-wall DNS, the gridded rough-wall DNS of cases 10_141 and 20_141, and the roughness-model DNS are shown in Figure 3. It can be seen that the model simulations produce a velocity profile that is similar to the true roughness case. The roughness function for case 10_141 is around $\Delta U^+_{model} \approx 4.8$ for the roughness models and 3.8 for the gridded roughness. There is little variation between the different filter scale models, with the roughness function changing by less than 5% for the different filter scales. For case 20_141, the roughness model produces a roughness function of $\Delta U^+_{model} \approx 8.6$ whereas the gridded roughness produces $\Delta U^+ = 7.1$. Again, relatively little variation between the filter scales used in the roughness model is seen. In the roughness model simulations, normalization is performed using a modified form of the friction velocity, $U_\tau = \sqrt{(\tau_w + F/A_w)/\rho}$, where both the shear stress at the wall, τ_w and the total forcing applied to the near-wall domain, F are included. These are exactly balanced by the pressure drop in the pipe.

The viscous and Reynolds stresses are shown in Figure 4. In agreement with Townsend's outer-layer similarity hypothesis, all the roughness model results collapse with the gridded-roughness and smooth-wall results in the outer layer, when normalized on the modified U_τ value. However, it can be seen in the insets of Figure 4 that the viscous stress for the model cases underestimates that of the gridded roughness until around $y^+ \approx 2.5h^+$. This results in U_x^+ being lower for the roughness model than the gridded roughness and hence the larger ΔU^+_{model} values. The Reynolds stress shows fair agreement; however the roughness model tends to slightly increase the peak Reynolds stress value, especially for case 20_141 where the model predicts a peak Reynolds stress value 5% greater than the gridded roughness.

Turbulence intensities for the azimuthal and streamwise directions are shown in Figure 5. It can be seen that the roughness model correctly enhances azimuthal velocity fluctuations close the wall, while damping streamwise fluctuations. The radial velocity fluctuations (not shown) exhibit a trend similar to the azimuthal fluctuations. All filter

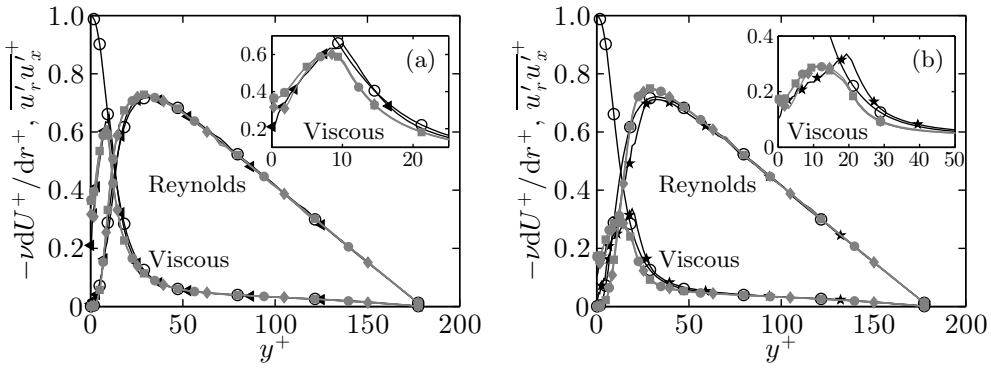

FIGURE 4: Viscous ($-\nu \mathrm{d}U^+/\mathrm{d}r^+$) and Reynolds ($\overline{u_r' u_x'}^+$) stress comparing the gridded-roughness DNS with the roughness-model DNS, for amplitudes $h^+ = 10$ (a) and $h^+ = 20$ (b). See Figure 3 for symbol definitions. Inset shows viscous stress close to the wall.

lengths have good agreement with the gridded roughness for $y^+ > h^+$, although the streamwise fluctuations are slightly damped. In the region of forcing ($0 < y^+ < h$), the model fluctuations drop below the gridded roughness. This is because of the no-slip boundary condition that is applied on the smooth wall at $y^+ = 0$ in the roughness model simulations. The finest filter scale, $\Delta_3 = \frac{1}{4}\lambda$ slightly enhances the fluctuations, however the improvement is not particularly significant.

The differences that are observed between the gridded roughness and the roughness model simulations are likely from the boundary conditions. In the roughness model, the wall is taken at $y^+ = 0$, and the gridded roughness trough within $-h^+ < y^+ < 0$ is not represented. This therefore changes the velocity at $y = 0$ because of the no-slip boundary condition employed in the roughness model simulations. Future efforts may involve changing the boundary location to see if this improves the roughness model.

In the roughness model simulations, the pressure drop across the length of the pipe is caused by two components; the real viscous drag acting on the smooth wall at $y = 0$, and the additional forcing term that is added over $0 < y \leq h$. Figure 6 shows the profile of the drag forces per unit wall-normal length, f, that are applied by the roughness model. Also shown are the drag forces per unit wall-normal length that are exerted by the roughness onto the fluid in the gridded-roughness DNS. If $F = \int f \, \mathrm{d}y$, then the total force applied to the domain $F_T = \int_0^h f \, \mathrm{d}y + F(y \leq 0)$ is exactly balanced by the pressure drop, where $F(y \leq 0)$ is either the viscous skin friction τ_w applied to the smooth wall at $y^+ = 0$ in the roughness model simulations, or the forcing in the trough ($-h^+ < y^+ < 0$) of the gridded roughness. Because the forcing term is proportional to $u_x|u_x|$, then it must be zero at the wall. The roughness model therefore has a lower forcing value close to the wall as compared to the gridded-roughness DNS results. The filter scale Δ_3 reaches zero at $y^+ > 0$ because of the artificial clipping of the forcing term employed. At this filter scale, ε is zero at $y = 0$ which would result in unbounded forcing (Eq. 2.6). It can be seen that the roughness model for case 20_141 results in a more accurate shear stress at the wall, when compared with the drag in the troughs of the gridded-roughness DNS. This suggests that the assumption that these two forces should be equal may be more appropriate for roughness with larger amplitudes, as the pressure force becomes

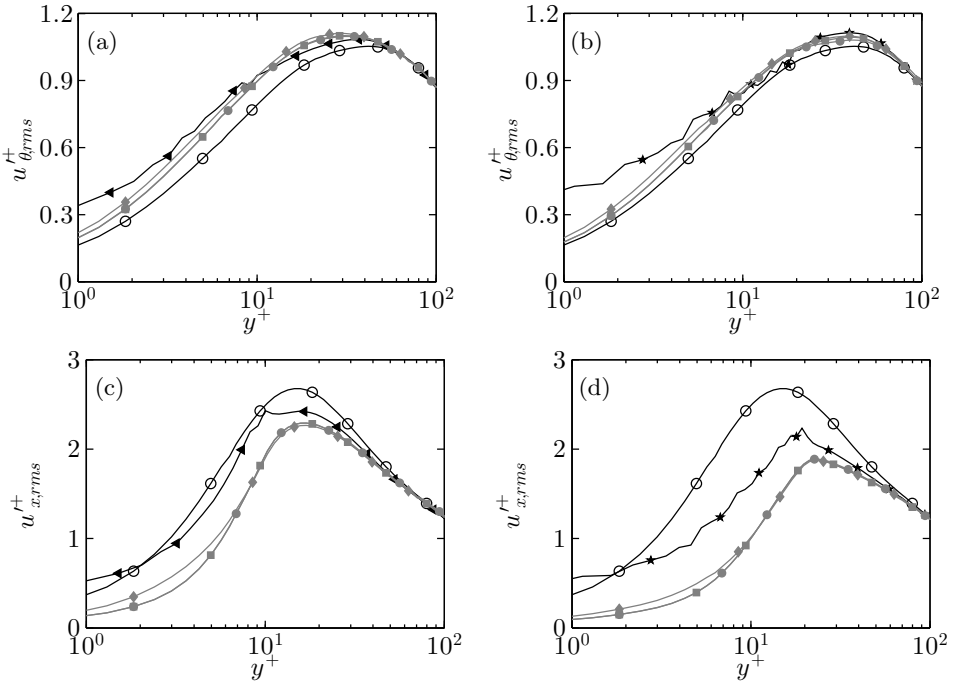

FIGURE 5: Azimuthal (a,b) and streamwise (c,d) turbulence intensities comparing the gridded-roughness DNS with the roughness model, for amplitudes $h^+ = 10$ (a,c) and $h^+ = 20$ (b,d). Refer to Figure 3 for symbol definitions.

dominant instead of the viscous forces. This may also suggest that the roughness model will improve with higher Reynolds numbers, where viscous effects become weaker.

3.3. *Flow structures*

A qualitative analysis is now performed to compare the time-averaged, spatially varying flow structures between the gridded-roughness DNS and the roughness-model DNS. Figure 7 shows the three components of velocity for case 10_141 and the three roughness model simulations, for a roughness height of $h^+ = 10$. Because the roughness model filter widths Δ_1 and Δ_2 result in no variation in θ or x, there is little variation in these components of velocity. Recall that filter width Δ_2 introduces only opposite-signed forcing in the azimuthal direction, which can be seen to introduce very weak azimuthal motions, even though the magnitude of this forcing is of order similar to the streamwise forcing. Only for the filter width Δ_3 do we begin to see similar secondary flow structures as in the gridded-roughness DNS case. Both the radial and azimuthal velocities contain the same features as the gridded roughness, however they are weaker in magnitude. The streamwise velocity has some of the same features as the gridded DNS, however it is located closer to the wall and is much weaker. Even with a relatively large filter and compared with the exact gridded roughness ($\Delta = \frac{1}{4}\lambda$), many of these time-averaged features can be seen. These time-averaged flows show that the spatial variation in drag coefficient for this filter scale allows for accelerating and decelerating flows, which enhances vortical flow regions in the modeled flow. It would seem that a finer filter scale of, say, $\Delta = \frac{1}{8}\lambda$ would be required to better resolve the streamwise features.

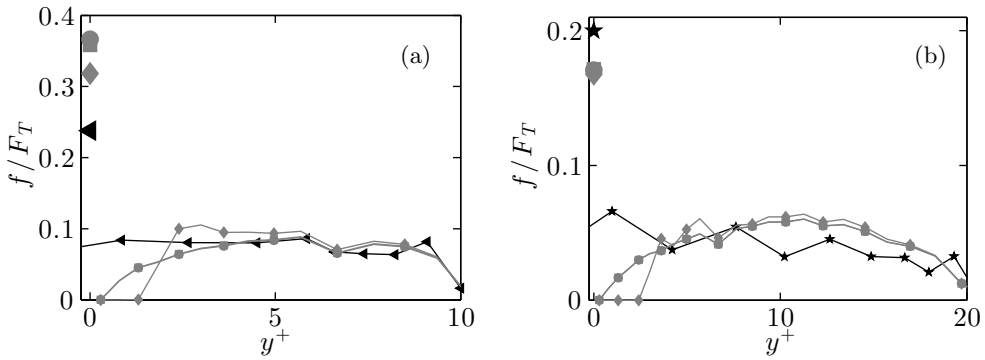

FIGURE 6: Streamwise forcing profile comparing the gridded-roughness DNS wall forces per unit wall-normal length with the roughness model applied forcing per unit wall-normal length, for amplitudes $h^+ = 10$ (a) and $h^+ = 20$ (b). The large symbols at $y = 0$, denoted $F(y \leq 0)$, correspond to the total force acting in the troughs ($y \leq 0$) for the gridded roughness, or the total viscous force on the smooth wall at $y = 0$ for the roughness model. $F_T = \int_0^h f\mathrm{d}y + F(y \leq 0)$ is the total force acting over the domain. Refer to Figure 3 for symbol definitions.

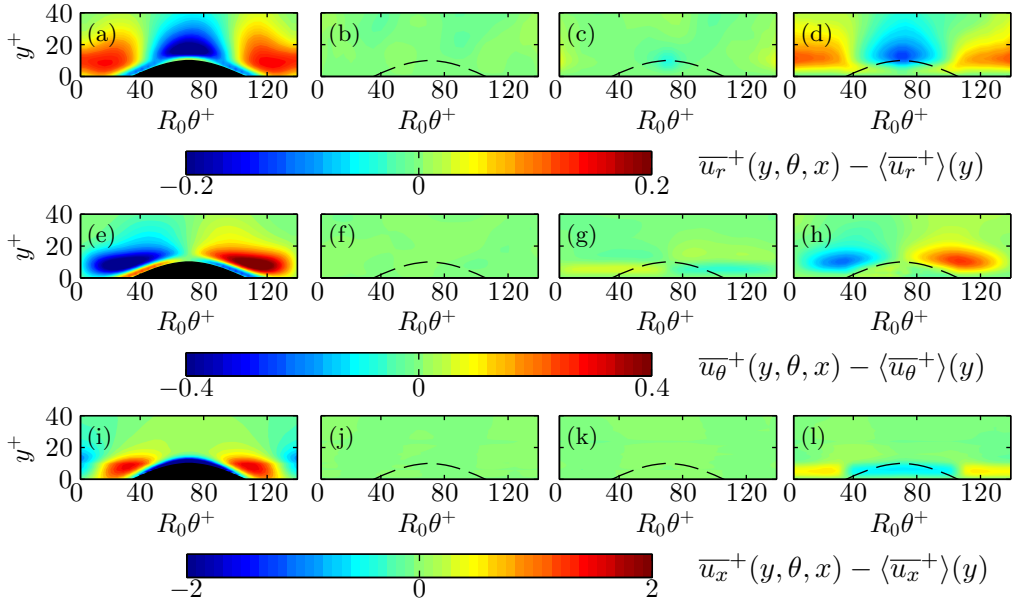

FIGURE 7: Time-averaged radial (a–d), azimuthal (e–h) and streamwise (i–l) velocity contours in the wall-normal–azimuthal plane for amplitude $h^+ = 10$. Gridded roughness (a,e,i), roughness models with filter lengths Δ_1 (b,f,j), Δ_2 (c,g,k) and Δ_3 (d,h,l).

4. Conclusions

A roughness model that applies a forcing term to the Navier–Stokes equations has been investigated, where the forcing term is based on the drag coefficient obtained from gridded-roughness DNS. Results from gridded-roughness simulations at $\mathrm{Re}_\tau = 180$ and $\mathrm{Re}_\tau = 540$ for matched roughness Reynolds numbers indicate that the drag coefficient C_D

does not change significantly. The model has been used in DNS of flow over a smooth wall at $\mathrm{Re}_\tau = 180$, with the comparison between the gridded roughness and model simulations showing fair agreement. The model provides a reasonable estimate of the roughness function, ΔU^+, as well as showing agreement for the viscous stress and turbulence intensities. Increasing the height of the roughness improves the results, possibly because the model better represents the increasing pressure drag rather than viscous drag effects. The difference in boundary conditions between the gridded roughness and the roughness model may explain some of the differences, as well as the low Reynolds number. Reducing the filter length used in the force coefficient shows some improvement in the turbulence intensities; however this improvement was negligible for the mean velocity profile. However, contours of time-averaged velocity showed that a filter scale of $\Delta = \frac{1}{4}\lambda$ had reasonable agreement with the gridded-roughness DNS for the radial and azimuthal velocities.

REFERENCES

Apte, S. V. 2004 A multilevel formulation to simulate particulate flows. *Annual Research Briefs*, Center for Turbulence Research, Stanford University, pp. 201–208.

Bhaganagar, K., Kim, J. & Coleman, G. 2004 Effect of roughness on wall-bounded turbulence. *Flow Turbul. Combust.* **72**, 463–492.

Breugem, W. P. & Boersma, B. J. 2005 Direct numerical simulations of turbulent flow over a permeable wall using a direct and a continuum approach. *Phys. Fluids* **17**, 025103.

Busse, A. & Sandham, N. D. 2012 Parametric forcing approach to rough-wall turbulent channel flow. *J. Fluid Mech.* **712**, 169–202.

Chan, L., MacDonald, M., Chung, D., Hutchins, N. & Ooi, A. 2014 A systematic investigation of roughness height and roughness wavelength in turbulent pipe flow in the transitionally rough regime. *J. Fluid Mech.* Under Review.

De Marchis, M. & Napoli, E. 2012 Effects of irregular two-dimensional and three-dimensional surface roughness in turbulent channel flows. *Int. J. Heat Fluid Fl.* **36**, 7–17.

Flack, K. A. & Schultz, M. P. 2010 Review of hydraulic roughness scales in the fully rough regime. *J. Fluid Eng.* **132**, 041203.

Nakayama, A., Hori, K. & Street, R. 2004 Filtering and LES of flow over irregular rough boundary. *Proceedings of the Summer Program*, Center for Turbulence Research, Stanford University, pp. 145–156.

Orlandi, P. & Leonardi, S. 2006 DNS of turbulent channel flows with two-and three-dimensional roughness. *J.Turbul.* **7**.

Park, G. I. & Moin, P. 2014 An improved dynamic non-equilibrium wall-model for large eddy simulation. *Phys. Fluids* **26**, 015108.

Raupach, M., Antonia, R. & Rajagopalan, S. 1991 Rough-wall turbulent boundary layers. *Appl. Mech. Rev.* **44**, 1–25.

Wang, M. & Moin, P. 2002 Dynamic wall modeling for large-eddy simulation of complex turbulent flows. *Phys. Fluids* **14**, 2043–2051.